Author Manuscript

Author Manuscript

Author Manuscript

Author Manuscript

HHS Public Access

Author manuscript

Optica. Author manuscript; available in PMC 2024 April 25.

Published in final edited form as:

Optica. 2023 November 20; 10(11): 1439–1451. doi:10.1364/optica.499927.

In vivo volumetric depth-resolved imaging of cilia metachronal waves using dynamic optical coherence tomography

Tian Xia[1], **Kohei Umezu**[1], **Deirdre M. Scully**[1], **Shang Wang**[2,3], **Irina V. Larina**[1,*]

[1]Department of Integrative Physiology, Baylor College of Medicine, Houston, Texas 77030, USA

[2]Department of Biomedical Engineering, Stevens Institute of Technology, Hoboken, New Jersey 07030, USA

[3] swang148@stevens.edu

Abstract

Motile cilia are dynamic hair-like structures covering epithelial surfaces in multiple organs. The periodic coordinated beating of cilia creates waves propagating along the surface, known as the metachronal waves, which transport fluids and mucus along the epithelium. Motile ciliopathies result from disrupted coordinated cilia beating and are associated with serious clinical complications, including reproductive disorders. Despite the recognized clinical significance, research of cilia dynamics is extremely limited. Here, we present quantitative imaging of cilia metachronal waves volumetrically through tissue layers using dynamic optical coherence tomography (OCT). Our method relies on spatiotemporal mapping of the phase of intensity fluctuations in OCT images caused by the ciliary beating. We validated our new method *ex vivo* and implemented it *in vivo* to visualize cilia metachronal wave propagation within the mouse fallopian tube. This method can be extended to the assessment of physiological cilia function and ciliary dyskinesias in various organ systems, contributing to better management of pathologies associated with motile ciliopathies.

1. INTRODUCTION

Motile cilia are microtubule-based dynamic organelles that protrude from the surface of cells in many different organisms and organ systems. They are evolutionally conserved; their diverse functions are essential for the survival and well-being of these organisms, and they are involved in a wide range of functions, including movement, sensory perception, and the maintenance of fluid flows. In microorganisms and some sea animals, periodically beating cilia enable locomotion to move the organism through the environment in a coordinated way [1–3]. In humans and other mammals, motile cilia are 200–300 nm in diameter and 5–10 μm in length. In early embryonic development, they are involved in the establishment of nodal flows, which are essential for left–right asymmetry [4]. They also cover epithelial surfaces in various parts of the body, including the respiratory tract, the middle ear, the kidney, the

* larina@bcm.edu .

Disclosures. The authors declare that they have no conflict of interest.

Supplemental document. See Supplement 1 for supporting content.

Author Manuscript Author Manuscript Author Manuscript Author Manuscript

brain, and the fallopian tubes, where they play important roles in moving fluids and particles along the epithelial walls [5–7].

The dynamics of cilia are highly regulated. The cycle of a ciliary beat consists of the faster effective stroke of the straightened cilium followed by the slower recovery stroke of the bent cilium (Fig. 1A). The coordination of the effective and recovery strokes between the neighboring cilia creates self-organized waves propagating along the surface, known as metachronal waves (MW). The MW is achieved by synchronizing the ciliary beat frequency (CBF) with a steady propagating phase shift relative to the neighbors within ciliated clusters. According to the modeling studies, the MW of motile cilia increases propulsion velocity more than three times in comparison to cilia that beat synchronously at the same frequency without phase delay [8,9]. It was shown that MWs emerge in response to hydrodynamical interaction between densely packed cilia [9,10]. Experiments in *Chlamydomonas* showed that elastic coupling through the cytoskeleton contributed to the flagellar synchronization [11,12]. Advancements in the numerical [9,13,14] and physical [8,15,16] modeling of ciliary behavior and activity provided insights into the effects of nonreciprocal motions of cilia on the surrounding viscous fluid.

Genetic abnormalities in motile cilia structures are associated with serious medical complications affecting developmental processes, respiratory function, brain function, and the reproductive system [17–19]. Large-scale genetic screens in mice revealed numerous cilia-related genes, including *Dnah5* and *Ift140*, which are associated with congenital heart disease [20]. Bustamante–Marin *et al*. demonstrated that the absence of *Gas2l2* causes a defective ciliary beat and impaired mucociliary clearance in the mouse airways [21]. Mee *et al*. reported that the gene associated with ciliopathy, *Hyls1*, is related to hydrolethalus syndrome, which is a perinatal lethal syndrome characterized by hydrocephalus and brain malformation [22]. Multiple genetic studies in patients demonstrate that these pathways are also affected in human ciliopathies [23].

Ciliated epithelial cells lining the lumen of the fallopian tube are known to play an essential role in reproduction [24]. Primary ciliary dyskinesia, a condition affecting cilia motility, is associated with fertility disorders in women and a higher incidence of ectopic pregnancies [25,26]. Previous investigations using genetic mouse models of cilia dysfunction in the fallopian tube have shown negative reproductive outcomes. Specifically, Yuan *et al*. demonstrated that mice deficient in microRNA clusters controlling multiciliogenesis had fewer and shorter cilia with weaker cilia beat frequency, as well as fewer live births [27]. Niwa *et al*. showed that mice lacking the microtubule-depolymerizing kinesin, KIF19A, were infertile due to elongated cilia and disrupted fluid flow [28]. Furthermore, studies in genetic mouse models revealed that disruption of a planar cell polarity gene, *Celsr1*, required for setting the orientation of ciliated cells in the fallopian tube of female mice, led to infertility [29], suggesting that collective and coordinated ciliary beating is essential for female fertility.

While the overall importance of motile cilia in reproduction is well recognized, what specific role they play in the fallopian tube and how ciliary dysfunction leads to fertility failures and pathological embryo implantation has not been defined and remains a

Author Manuscript Author Manuscript Author Manuscript Author Manuscript

controversial subject [30,31]. There is a classic belief that the primary function of fallopian tube cilia is to transport oocytes and preimplantation embryos to the uterus for implantation. However, a recent *in vivo* imaging study suggested that this role is unlikely because the revealed movements of oocytes and embryos were not compatible with cilia-generated dynamics. Instead, it was suggested that rather than facilitating the directional transfer of oocytes and embryos, the motile cilia generate local flow fields to steer luminal contents from epithelial walls, and cilia-generated flows were suggested to navigate spermatozoa in their journey to the fertilization site. It was also reported that ciliary beat frequency (CBF) changes dramatically over the course of the estrus cycle and pregnancy [32], but how these changes translate into fallopian tube function and how ciliary roles change during these processes is not clear. Despite the recognized clinical importance, the capability to answer these and other questions about ciliary role in the fallopian tube is limited by the current imaging capability to visualize cilia and cilia-coordinated function.

Traditionally, the ciliary dynamics is visualized using high-speed video microscopy in organisms with exposed ciliated surfaces, or *ex vivo*, which involves dissecting the organ of interest and exposing the ciliated surface for the imaging [33–35]. However, the biochemical and biomechanical environment of the cilia undergoes significant disruption during this process, leading to an inaccurate interpretation of the physiology.

Optical coherence tomography (OCT) has been gaining recognition as a promising tool for motile cilia investigation *in vitro, ex vivo, and in vivo*. This microscopic imaging technique is capable of high-speed, depth-resolved imaging with an imaging depth of 1–2 mm in an optically scattering medium. Over the last decade, there has been significant progress in OCT-based technologies for cilia analysis. The Tearney group pioneered μOCT with a 1 μm axial resolution to resolve subcellular structures [36], which allowed them to visualize the cilia beat pattern, including the effective and recovery strokes, at the level of individual cilia [37]. Quantitative measures based on μOCT were also developed, not only on assessing the ciliary dynamics itself but also on the mucociliary transport [37,38]. Quantitative measures, including the CBF, the angular range of the cilia effective stroke, and the motile ciliary region, have enabled a range of studies on various ciliated samples, from *in vitro* cell cultures [39,40], to *ex vivo* respiratory tissues [41,42], to *in vivo* airway in the porcine model [43]. Notably, the recent demonstration of μOCT for *in vivo* human intranasal imaging is promising in transforming the clinical care of respiratory conditions, such as cystic fibrosis [44]. The ultra-high resolution of μOCT is achieved using a light source with a very broad bandwidth [36]; however, due to the limited pixels in the line-scan camera of the OCT system, this leads to a relatively short depth range that restricts the investigation to the exposed ciliated surfaces.

While the cilia are below the resolution of traditional OCT, their beat creates intensity fluctuations in OCT images, allowing the use of OCT to image the motile cilia without having the 1 μm axial resolution. The Oldenburg group first employed the OCT intensity variation produced by the movement of cilia to reveal the cilia location and measure the CBF on the *ex vivo* and *in vitro* models of mouse trachea [45]. Taking this further, our group developed *in vivo* depth-resolved, micro-scale mapping of the cilia location and CBF in the mouse fallopian tube by pixel-wise frequency analysis of intensity fluctuations in OCT

Author Manuscript Author Manuscript Author Manuscript Author Manuscript

images [32]. The Hendon group implemented this method to map the cilia location, CBF, and the resulting mucus flow in *ex vivo* human tracheo-bronchial samples [46]. While not in application to cilia analysis, the Grieve group developed a dynamic full-field OCT approach, which allowed them to differentiate cell types in *ex vivo* samples based on frequency analysis in pixel fluctuations due to subcellular motility [47,48]. The periodic up-and-down movement of cilia is also reflected in the change of phase from the interferometric OCT signal, which was first demonstrated by the Chen group [49]. This method was implemented with spectrally encoded interferometric microscopy in extracted flattened samples of the porcine oviduct and rabbit tracheal for mapping of CBF [50,51] and MW [52]. The phase analysis has the advantage of high sensitivity; however, this method currently requires the ciliated surface to be flattened and positioned perpendicularly to the scanning beam.

Probing ciliary function with OCT was also achieved indirectly through imaging the cilia-driven fluid flow [53]. A series of OCT-based particle tracking velocimetry methods were developed to quantitatively map and evaluate the flow fields created by cilia [54–56] and were used to study the cilia-related phenotypes in the *Xenopus* model with different types of perturbations [57] and from the mouse trachea with hyperoxia [58].

Despite all the developments in imaging technologies, none of the previous methods is applicable to the orientation-independent analysis of cilia coordination through tissue layers. Here, to the best of our knowledge, we present a novel OCT-based quantitative approach for depth-resolved imaging and quantitative analysis of cilia MW, which can be performed volumetrically. The method relies on the spatiotemporal mapping of the phase from the ciliary beat, which is derived from variations in OCT image intensity in corresponding pixels. The propagation of the cilia MW can be directly visualized, and the wave velocity can be measured. We validated the new method using bright-field video microscopy and implemented it to investigate the effect of temperature on MW velocity. We implemented two alternative acquisition protocols. MW imaging was performed as 2D + time scanned volumetrically, to provide MW velocity measurements over a large field of view, such as the whole oviduct ampulla, but with MW velocities restricted to the imaging plane orientation. We also implemented direct volumetric 3D + time cilia MW mapping to reveal MW propagation in any direction, but over a smaller field of view. The female reproductive system is positioned deep within the body, which limits direct imaging access. However, using an intravital imaging approach, which involves the implantation of a chamber with a transparent aperture on the back of the female mouse, allows for *in vivo* imaging of the fallopian tube with OCT (Fig. 1B). Here, we applied the newly developed method for MW analysis in combination with this intravital *in vivo* approach, which allowed us to visualize and quantify cilia MW within the lumen of the mouse fallopian tube *in vivo* within the natural physiological environment. This study presents the first quantitative method for imaging the cilia MW through tissue layers and sets a platform for the investigation of the ciliary role in reproductive physiology and reproductive disorders *in vivo*, as well as in other organ systems.

Author Manuscript Author Manuscript Author Manuscript Author Manuscript

2. RESULTS

A. Method for Cilia Metachronal Wave Imaging with OCT

Beating cilia create periodic intensity fluctuations in OCT images, which carry information about the frequency and the phase of ciliary beating at corresponding pixels. The metachronal wave is created by a shift in the phase of beating between neighboring cilia. Our method allows for direct visualization and quantifications of metachronal waves by mapping the phase of OCT intensity fluctuations due to ciliary movement in space and time. The algorithm of the method is presented in Fig. 2. The first step (Figs. 2A and 2B), mapping cilia locations and CBF on corresponding spatial pixels was described in detail in our previous publication [32]. Briefly, OCT time-lapse imaging is performed over a ciliated sample; then the fast Fourier transform (FFT) is performed on the temporal OCT intensity profile to reveal the spectrum of intensity fluctuations for each spatial pixel. The dominant peak in the spectrum for each pixel, passing the thresholding and masking, represents cilia beat frequency (CBF) at the corresponding location. In the presented example, the imaging frame rate was set to 100 Hz. According to the Nyquist–Shannon sampling theorem, the maximum measurable frequency with these settings is 50 Hz, which is sufficient to resolve the CBF in most organs and model organisms [59], including the mouse fallopian tube [60–62]. The number of images used for each FFT was 128 over 1.28 s, which resulted in a spectral resolution of ~0.78 Hz for the frequency measurement. To increase the spectral resolution, potentially, the acquisition time (and the number of images) for FFT can be increased. Because we do not expect CBF to exceed 20 Hz [60–62], all signals at the frequency window of 25–50 Hz were taken as noise and used to set the amplitude threshold for the whole frequency range, as an average plus three standard deviations. The frequency peaks above the threshold are considered as the CBF signal in corresponding pixels (Fig. 2B). The lack of similar periodic motion in non-ciliated parts of the sample, such as the mucosa, creates the contrast for imaging the cilia location.

The cilia metachronal wave analysis is performed by mapping phases across pixels one frequency at a time. Following the CBF mapping step, the dominant CBF is selected based on the higher number of pixels exhibiting this beat frequency in the area of analysis. Regions exhibiting different dominant frequencies can be processed separately. A binary mask for the selected dominant frequency is created to include all pixels in which the selected frequency is over the defined threshold (Fig. 2C), and the phase of this selected frequency from FFT is mapped on the corresponding pixels (Fig. 2D).

The phase delays between neighboring pixels produce an instantaneous snapshot of the metachronal wave across the sample, where one complete phase wrap corresponds to the wavelength of the metachronal wave. If the whole phase wrap is clearly identifiable within the snapshot, one can calculate the velocity of the metachronal wave based on the frequency and the wavelength. This part of the proposed algorithm was previously used for the evaluation of metachronal wave velocity in microscopic imaging [35]. However, due to the relatively low resolution of OCT and the rather small size of ciliated patches within 2D OCT cross-sections, the direct quantification of the MW from such snapshots from OCT data is extremely challenging. To overcome this challenge, we expanded this analysis to dynamic

Author Manuscript Author Manuscript Author Manuscript Author Manuscript

visualization of MWs (Fig. 2E). For that, the FFT analysis and the phase mapping for the same frequency are performed repeatedly with a sliding window over time. While each phase map for each time point is reconstructed based on images acquired at different time points, the sliding window approach produces dynamic visualization of the MW propagation in space over time. Figure 2F shows a volumetric view of the 2D + time phase dataset with a cross-section going along the ciliated grooves of the oviduct. The metachronal wave produced by the coordinated ciliary beating is seen as a sequence of tilted wavefronts in the cross-sectional plane of time versus space. The dynamic visualization of the phase provides direct visualization of the metachronal wave propagation, while the angle of the wavefront tilt, or the distance traveled by the wavefront over time, reveals the MW velocity along the imaged plain in each ciliated location of the image (Visualization 1 and Fig. 2F).

B. OCT Metachronal Wave Analysis as 2D + time Mapped Volumetrically

We expanded the described method to mapping the cilia metachronal waves volumetrically as 2D + time sequence. For that, we acquired OCT time-lapses over the area of ~1.27 mm × 95 μm at the frame rate of 100 Hz as a single continuous spatially dense volume of 10,000 frames, 1000 A-lines/B-scan. Such settings provide B-scan spacing of ~9.5 nm, and each consecutive 128 frames (for FFT) can be treated as acquired from the same spatial location because the total displacement over this range of frames is less than the spatial resolution of the OCT imaging system (4 μm). The 2D + time phase and the metachronal wave mapping as described above was performed repeatedly in a form of a sliding window over the whole volume with a step of 10 frames. The metachronal wave visualization is only meaningful within each imaging plane of the volume and represents the metachronal wavevector component along that plane.

This volumetric scanning approach and imaging settings were successfully used to image metachronal waves within large portions of the mouse fallopian tube, though luminal grooves of the ampulla portion, which are known to be densely covered by cilia, *ex vivo* (Figs. 3 and 4) and *in vivo* (Fig. 5). The volumetric 2D + time scanning provided more complete datasets and allowed for flexibility in locating specific regions of interest for validation based on the corresponding OCT volumetric structural images.

C. Validation of the OCT Metachronal Wave Analysis Using Bright-field Video Microscopy

The bright-field video microscopy is the primary method for cilia metachronal wave analysis [35,63]. In this case, the ciliated surface has to be directly exposed for imaging and oriented within the focal plane. The beatings of motile cilia can be directly visualized with bright-field imaging at high magnification, and the phase of the ciliary beat at each location can be extracted through FFT, similarly to the first two steps of our approach [35,63]. The metachronal wave velocity is usually quantified based on the frequency and the phase wrap distance (MW wavelength) within the phase maps. Our new method for metachronal wave quantification is applicable to both OCT and bright-field video microscopy images. The metachronal wave velocity measurements using the traditional approach based on the phase wrap length and frequency and our new method shown in Fig. 2 are equivalent by the principle, which we also confirmed experimentally using bright-field video microscopy

Author Manuscript Author Manuscript Author Manuscript Author Manuscript

of extracted ciliated samples. Hence, we used the bright-field video microscopy-based metachronal wavefront mapping with our method for the validation of OCT measurements.

To validate the OCT-based metachronal wave measurements, the imaging was performed sequentially with OCT and bright-field microscopy on the same locations of the same ciliated samples. Because the bright-field video microscopy requires the ciliated surface to be directly exposed for imaging, mouse fallopian tubes were dissected out and opened up micro-surgically with luminal epithelial surfaces facing up. The OCT imaging captured data volumetrically (Fig. 3A), while the bright-field video microscopy showed only the top view of the sample (Fig. 3E). The structural details of the OCT volumetric rendering in the top view were used to locate the same region for the two modalities, and the metachronal wave measurements with OCT were taken from the top surface of the sample in the corresponding in-depth cross-sections (Fig. 3B). Following the CBF mapping (Figs. 3C and 3G), the phase at the same dominant frequency was mapped over space and time in the same location for two modalities, revealing the metachronal wavefront propagation at comparable velocities (Figs. 3D and 3H).

The overall distributions of metachronal wave velocity measurements with two modalities fall in a similar range (Fig. 3I). The analysis of the paired metachronal wave measurements (Fig. 3J) revealed a statistically significant correlation between the modalities ($p < 0.05$). Each pair of measurements are shown in Table S1. While the overall distribution of the measurements was similar, we observed slightly higher values for OCT measurements in comparison to bright-field video microscopy (slope of 1.2). Such a difference was expected because bright-field video microscopy relies on top-view projections for analysis and tends to slightly underestimate the MW velocity if the ciliated surface is not perfectly parallel to the imaging plane. In contrast, the OCT relies on in-depth cross-sections and tends to overestimate the MW velocity if the metachronal wavefront is not perpendicular to the imaging plane. In addition, since the measurements with two modalities were acquired sequentially, some biological variability was expected. However, the high level of correlation between the modalities demonstrates that imaging planes were indeed oriented largely along the MW propagation directions, as intended, and validates the OCT-based method for visualization and quantitative assessment of cilia metachronal wave.

D. Effect of Temperature on Cilia Metachronal Wave Velocity

It is well known that temperature affects CBF. Whether temperature also affects cilia metachronal wave propagation has not been investigated before, to the best of our knowledge. We implemented the new OCT-based imaging method to study the effect of temperature on the cilia metachronal wave velocity in mouse fallopian tube *ex vivo*. OCT imaging of extracted intact fallopian tube samples was performed at the same locations at three temperature settings: 20°C, 30°C, and 37°C (Fig. 4A). The structural OCT images at these three temperatures (top row in Fig. 4A) clearly show longitudinal luminal grooves, which are known to be highly ciliated, and confirm the same spatial location for the analysis. As expected, the color-encoded CBF mapping showed an overall increase in CBF with temperature, which is seen by the gradual change of colors from blue/green toward green/yellow as the temperature changed from 20°C to 37°C (second row of Fig. 4A). The

Author Manuscript Author Manuscript Author Manuscript Author Manuscript

temperature-dependent CBF increase in these images was also confirmed quantitatively (Fig. 4B), demonstrating the shift in the peak of CBF distributions from ~4.5 Hz at 20°C to ~7.5 Hz at 30°C, to ~12 Hz at 37°C. This result is in agreement with the previous study of ciliary dynamics in the upper airway [49]. The metachronal wavefront propagation analysis (bottom row of Fig. 4A) revealed a dramatic increase not only in CBF, but also in metachronal wave velocity with temperature increase. This result was confirmed through statistical analysis of metachronal wave velocities measured in multiple samples (Fig. 4C). Since the fallopian tube samples used for bright-field microscopy had to be opened up micro-surgically, which disrupts the luminal microenvironment, the measurements of the metachronal wave velocity were lower than those acquired with OCT, but the temperature-dependent change was also detected. These results provide the first, to the best of our knowledge, quantitative confirmation of temperature dependence of metachronal wave velocity and demonstrate the importance of OCT-based depth-resolved investigation of ciliary dynamics in comparison to classical bright-field microscopy, which requires disruption of the fallopian tube luminal microenvironment.

E. *In Vivo* Application of OCT-based Cilia Metachronal Wave Analysis

The major advantage of the OCT-based metachronal wave analysis is its capability to implement it *in vivo* to study ciliary function in intact organs through tissue layers. We previously established an *in vivo* OCT imaging of the mouse reproductive system through an intravital window, which was successfully used for prolonged and longitudinal studies [64,65]. This intravital imaging approach was implemented here for *in vivo* metachronal wave analysis in a mouse fallopian tube. To avoid movement artifacts caused by animal breathing, the reproductive system is positioned on specially designed prongs of the intravital window, fixed with clamps to the imaging stage. To reduce any potential remaining movement artifacts, imaging was performed at a faster frame rate of 200 Hz, while the same number of frames (128) was used for each FFT measurement. At these settings, each FFT measurement was acquired over 0.64 s, while the MW propagation tracking was done in less than one second. The algorithm requires cilia to remain within the same pixel of resolution for the duration of MW tracking. The bulk movement resulted in obvious disruption of MW patterns; the fragments of the time series associated with the bulk movement were disregarded. An example of *in vivo* metachronal wave analysis is shown in Fig. 5. The overall top view of the fallopian tube grove is shown in Fig. 5A, labeling the location of the slice where the ciliary analysis was performed. Within the 2D + time dataset (Fig. 5B), we located the position containing the ridge of ciliated mucosa folds (Fig. 5C) for metachronal wave analysis. The corresponding CBF map, a spectral mask, and phase at 14.1 Hz are shown in Figs. 5D–5F, respectively. The phase mapping over space and time revealed the metachronal wave velocity of 350 μm/s along the luminal grove (Fig. 5G), while no metachronal wave propagation was detected perpendicular to the grove, suggesting the overall direction of the wave propagation along the grove. To the best of our knowledge, this is the first *in vivo* analysis of the cilia metachronal wave in a mammalian model.

F. Direct Volumetric Imaging of Cilia Metachronal Wave Propagation

We achieved direct 3D + time OCT metachronal wave imaging by reducing the transverse scan area and pixel density and increasing the A-line and volumetric acquisition rates (Fig.

Author Manuscript Author Manuscript Author Manuscript Author Manuscript

6). Although the transverse scan area was relatively small, this approach provided the flexibility to analyze the wave propagation in any direction. The imaging was performed at 100 A-lines/B-scan, 30 B-scans/volume covering the region of 127 μm × 48 μm × 1.5 mm (depth) at a direct volume rate of 41.7 Hz. Figure 6A shows the size and the location of the imaged fragment of the mouse fallopian tube *ex vivo*. Based on the dominant frequency and frame position in the volume, the phase was corrected to compensate for the volumetric scan time. The structural OCT volumetric rendering of the 3D + time scanned region (Fig. 6B) shows the luminal grooves within the lumen. Corresponding volumetric CBF mapping revealed that the grooves are densely covered by cilia (Fig. 6C), with a strong presence of 5.2 Hz frequency all over the grooves (Fig. 6D). Depth-resolved volumetric phase propagation was detected all over the ciliated grooves (Visualization 2). The cilia MW analysis was performed along two orthogonal lines labeled in Fig. 6E; the first one was placed across, and the second one was along the visible wavefront. The temporal phase mapping along these lines indeed revealed the MW propagation along the direction of the first line (Fig. 6F), but not the second one (Fig. 6G), demonstrating that the MW indeed propagated in the direction of the first line.

3. DISCUSSION

This study presents the first quantitative method for imaging the cilia beat coordination through tissue layers. Our approach can map and quantify the cilia location, CBF, and the MW propagation over the structural image at a micro-scale spatial resolution with a depth-resolved field of view that covers the entire ampulla of the fallopian tube. Because the method takes advantage of the speckles produced by the interference of light, no exogenous contrast agents are required. The approach could be used as 2D + time scanned volumetrically over a large field of view to map MW velocity components along the plane of scanning. Alternatively, direct volumetric imaging (3D + time) can be implemented over smaller areas to visualize MW propagation in any direction. Our studies revealed that not only CBF, but also the MW velocity are highly dependent on temperature, demonstrating high sensitivity and large dynamic range for our method. The newly established method was successfully implemented *in vivo* using an intravital imaging approach to visualize and quantify MW propagation in the lumen of the mouse fallopian tube.

Because mammalian reproduction takes place deep inside the body, the cilia function in the fallopian tube is not well understood and is open to conjecture, thereby limiting the progress of infertility treatments. Our new method in combination with the intravital imaging approach enables live dynamic investigation of ciliary dynamics in correlation with cilia-induced flow patterns, structural changes of the fallopian tube, and tracking the movement of oocytes and preimplantation embryos. Mouse models provide an irreplaceable resource for healthcare with thousands of genetic and epigenetic models available to study human diseases, including over 300 genetic mouse models associated with fertility defects. Investigations of the ciliary role in fertility failures in these models will inform human reproductive healthcare strategies.

There is also a translational potential for this method in reproductive research. Fiber-based OCT probes guided through the fallopian tube (falloposcopes) are currently being developed

Author Manuscript Author Manuscript Author Manuscript Author Manuscript

for cancer diagnostics and screening [66,67]. OCT fiber-based falloposcopes are expected to enter clinical trials to become standard clinical practice within a few years. New methods developed in this study for dynamic cilia analysis can potentially be directly adapted for diagnostic purposes in clinics, and novel scientific findings in mice could be corroborated in humans, toward better female reproductive health management.

Motile cilia are involved in the regulation of physiological processes all over the body, and the method presented for depth-resolved imaging of cilia MW through tissue layers has the potential for extending the assessment of ciliary dyskinesias to various organ systems. For example, with the recent advancements in endoscopic OCT imaging of the upper airway [68–70], this method can be applied for investigation and potential diagnostics of pathologies in the coordination of ciliary activity in the respiratory system. Another potential application is related to motile cilia function in the regulation of fluid flows within brain ventricles [6]. Ciliary analysis with OCT in adult brains should be possible *in vivo* in small animal models, such as zebrafish. In mice, embryonic brain imaging could be performed *in vivo* through the uterine wall with OCT [71,72]. Analysis of coordinated ciliary function in the embryonic brain in normal and pathological conditions in genetic mouse models could provide new insights toward congenital and developmental neurological disorders. Our studies investigating the effect of temperature on cilia MW revealed dramatic changes in MW velocity, as well as high sensitivity and a large dynamic range for MW detection with our approach. This suggests a potential for our method to study the effects of environmental factors, substances of abuse, and toxins in different organ systems, some of which are already known to affect cilia function [73,74].

This study introduces a new approach and demonstrates its potential for biomedical applications. However, it is currently associated with limitations and will benefit from multiple further advancements. Our method for 2D + time volumetric scanning of cilia MW has the advantage of covering a large volume; however, the MW measurements are only meaningful within each plane. If the metachronal wavefront propagation direction is not aligned to the imaging plane, the actual and the measured velocity values are correlated as

$$V = V_{\text{mes}} * \cos(\alpha),$$

where V is the actual MW velocity, V_{mes} is the measured MW velocity, and α is the angle between the axis of the metachronal wavefront propagation and the line, where MW was measured. To increase the chances of imaging along the MW, we attempted to orient the imaging plane along the grooves of the fallopian tube lumen. We also ensured consistent sample orientation for imaging over different temperatures. However, we acknowledge that due to the complexity of the fallopian tube, the MW velocities measured as 2D + time are likely overestimated. This artifact is avoided by the direct 3D + time scanning, which reveals metachronal wavefront propagation in any direction volumetrically, although over a much smaller volume. Due to different spatial scales, 2D + time and 3D + time mapping could be used as complementary. Alternatively, an automated tiled 3D + time acquisition covering a larger area, such as the whole ampulla of the fallopian tube, could be implemented. Another approach could involve the acquisition of two orthogonal 2D + time datasets scanned over

Author Manuscript Author Manuscript Author Manuscript Author Manuscript

the same volume to reconstruct the vector field of cilia MW velocities in space. The major limitation for increasing the scan size of direct 3D + time imaging is the OCT scan rate. Implementation of faster OCT systems, which are actively being developed [75], would also be beneficial for direct volumetric metachronal wavefront imaging with higher resolution and over larger areas.

Here, we performed the FFT analysis for CBF mapping based on 128 frames, which at 100 Hz imaging rate resulted in a relatively low spectral resolution of 0.78 Hz. To reduce the effect of movement artifacts, the imaging frame rate was increased to 200 Hz for the *in vivo* study. With 128 frames used for each FFT analysis, these settings resulted in a spectral resolution of 1.56 Hz. Such settings allowed for faster measurements of the metachronal wave, 0.64 seconds per each FFT measurement, and MW velocity measurement in less than a second. Such fast measurements were highly beneficial for *in vivo* imaging but at the expense of spectral resolution. We found it to be sufficient for the purpose of the study. However, if the study demands, the spectral resolution could be improved by increasing the time interval used for FFT analysis with the same sliding-window-over-time approach for MW propagation mapping, as presented here. Increasing the spectral resolution and frame number for analysis will improve the quality of the MW mapping, particularly at lower CBF, but will require a longer acquisition and will be more susceptible to movement artifacts. These parameters would need to be balanced based on specific experiments.

In this study, the phase of the ciliary beating was defined from FFT analysis of structural OCT intensity fluctuations. Going further, it is important to explore whether employing the phase (Doppler shift), as demonstrated before by Jing *et al.* for CBF mapping [49], in addition to the structural OCT intensity, would be beneficial. The ciliary beat cycle consists of a faster beating stroke of the extended straight cilium followed by a slower recovery stroke while the cilium is bent. OCT Doppler shift measurements are likely to be more sensitive to distinguishing specific phases of the ciliary beat, particularly in *en-face* orientation. However, OCT phase measurements are much more sensitive to bulk movements and tissue orientation and might or might not be advantageous for cilia metachronal wavefront propagation analysis *in vivo*.

Integration of the presented cilia MW imaging with other OCT-based functional methods might provide a synergistic advantage in studying motile cilia. For example, OCT-particle-tracking velocimetry has been previously developed for volumetric mapping of flow fields as a measure of motile cilia coordination and function [55]. Simultaneous imaging and co-registration of the volumetric MW fields and cilia-generated flows will provide a tool for studying the mechanism and regulation of the transport function of motile cilia.

Several computational modeling studies are currently underway to simulate ciliary dynamics, coordinated behaviors, and regulation of MW parameters, in relation to the flow fields [9,14,76]. However, the lack of experimental data for these parameters in the physiological environment has limited opportunities for calibration and validation of computational models, hindering further advancement. Computational modeling of cilia is a particularly challenging task in organs that are concealed from direct observation by layers of tissue, structurally complex and dynamic, and filled with non-homogeneous fluids, such

Author Manuscript Author Manuscript Author Manuscript Author Manuscript

as the fallopian tube. Spatially and temporally resolved measures of ciliary coordination in relation to fluid dynamics in their native context, now accessible with the presented method, will inform the numerical models and empower a more thorough investigation of ciliary function.

The nature-inspired robotic designs have gained increasing attention and have proven successful in undertaking challenging tasks [77,78]. Among other designs, artificial cilia have been implemented for controlled object movement and generating fluid flow [79,80]. Therefore, insights into coordinated ciliary activity implemented by nature *in vivo* could be useful in advancing the design of cilia-based robotics.

In summary, we presented the first quantitative method for depth-resolved imaging of cilia metachronal waves through tissue layers. This method is uniquely suited for the investigation of ciliary function within the fallopian tube in mouse models *in vivo*, volumetrically, through layers of tissue. Potentially, this method can be extended to the assessment of ciliary dyskinesias in various organ systems, toward better prevention, diagnostics, and treatment of ciliopathies.

4. METHODS

A. Mouse Manipulations for *Ex Vivo* and *In Vivo* Imaging

All animal procedures have been approved by the Institutional Animal Care and Use Committee at Baylor College of Medicine, and all experiments followed the approved guidelines and regulations. Experiments were performed on wild-type CD-1 female mice (age >6 weeks, Strain Code 022, Charles River).

For *ex vivo* experiment, the fallopian tubes together with the attached ovary and a part of the uterine horn were freshly dissected from euthanized mice into PBS solution at room temperature (20°C). For the validation study, the lumen of the fallopian tube was carefully opened through micro-surgical dissection under the dissecting microscope. To ensure consistency in tissue orientation between the two imaging modalities, the fallopian tube samples were carefully pinned down to the bottom of a petri dish, while exposing the ciliated lumen in a relatively flat orientation. The tissues were emerged in PBS and maintained at room temperature, unless noted otherwise. The ciliated samples were imaged first using bright-field video microscopy, and right after with OCT.

To study the effect of temperature on cilia dynamics, the fallopian tube together with the attached ovary and a part of the uterine horn were freshly dissected from euthanized mice into PBS solution at room temperature (20°C). The intact organs were placed in 60 mm Petri dish filled with PBS on the top of a heating platform (Homeothermic controller type 874, Hugo Sachs Elektronik) on the OCT imaging station. The temperature was monitored by probing the PBS solution in another dish placed side-by-side with the experiment dish. The temperature was increased in steps, starting from room temperature of 20°C to 30°C, then 37°C. OCT imaging was performed at each temperature setting.

Author Manuscript Author Manuscript Author Manuscript Author Manuscript

In vivo imaging of the fallopian tube was done through an intravital approach as described in [64,65]. To bypass the skin and muscle and provide imaging access to the reproductive system, the approach involved the implantation of a window on the back of the mouse. The windows are produced in the lab on a high-resolution 3D printer (Form2, gray resin, Formlabs) The window design featured a clear aperture of 10 mm in diameter for optical imaging access. The mouse was anesthetized by isoflurane inhalation and maintained on a 37°C heating platform. The site of implantation was processed for hair removal and skin disinfection. A circular part of skin tissue with ~1 cm diameter was removed, and the window was sutured to the edge of the skin through 14 eyelets along the rim using 4–0 Nylon suture. Once the window frame was implanted, the muscle layer underneath the window aperture was cut for a ~2 mm incision to expose the reproductive organs. The ovary, the oviduct, and part of the uterus were gently stabilized by securing the fat pad associated with the ovary onto the window tissue holders/prongs using a tiny droplet of surgical glue. The window aperture was closed by a 12-mm-diameter circular cover glass and secured with an O-ring. The animals were maintained under isoflurane anesthesia for the duration of imaging. The window was stabilized in space with clamps to successfully eliminate bulk movement artifacts caused by mouse breathing.

B. Bright-field Microscopic Imaging

Bright-field microscopic imaging of the *ex vivo* oviduct was performed using a Zeiss Imager A2 microscope equipped with a digital camera (AxioCam 702 mono, Zeiss). The time series of the bright-field microscopic images from the oviduct were taken with 40 × magnification at a frame rate of 88 Hz or 100 Hz. The acquired 2D images have the pixel scale of 0.147 μm for both transverse directions.

C. OCT System and Imaging

We used a house-built spectral domain OCT system. The system employed the supercontinuum laser (NKT Photonics) with a central wavelength of ~800 nm and a bandwidth of ~100 nm. The system used a fiber-based Michaelson interferometer; the interference of light from the reference and sample arms was directed to a spectrometer based on a 250 kHz e2V OctoPlus camera (Teledyne Technologies Inc.). Fast Fourier transform was used to obtain the OCT intensity A-line from equally *k*-spaced interference fringes. The system provided an A-line rate of up to 250 kHz and had an axial and transverse resolution of ~4 μm and an imaging depth of ~1.5 mm. To perform transverse scanning, we used a set of galvanometer mirrors (GVS012, Thorlabs Inc.), which provide high flexibility in adjusting the scanning size and pixel density.

Structural volumetric OCT datasets over a large field of view, covering the whole fallopian tube ampulla *ex vivo* and *in vivo*, were acquired as a single volume of 1000 × 1000A-lines over 1.27 × 0.95 mm.

For 2D + time OCT images acquired volumetrically *ex vivo* and *in vivo*, datasets were acquired as a single spatially dense volume of 1000 × 10,000A-lines over 1.27 × 0.095 mm, which resulted in a spatial step of 9.5 nm between frames. The frame rate was 100 Hz

Author Manuscript Author Manuscript Author Manuscript Author Manuscript

for the *ex vivo* experiment and 200 Hz for the *in vivo* experiment, which was achieved by increasing the A-line rate.

The datasets for direct volumetric cilia MW tracking were acquired as 100 × 30A-lines over 0.127 × 0.048 mm. The exposure time for each A-line was set to 3.3 μs with an A-line period of 4.0 μs (250 kHz A-line rate). The galvanometer reset time between frames was 0.4 ms, which resulted in a frame rate of 1,250 Hz and a volume rate of 41.7 Hz. Each dataset was acquired as 300 volumes, which took 7.2 s. The FFT was performed over 128 volumes and the MW tracking was performed using the same sliding window approach over time as described above.

D. CBF Mapping and Cilia MW Analysis

As the first step to cilia MW analysis for both imaging modalities, bright-field video microscopy and OCT, CBF mapping was performed to identify pixels with periodic intensity variation in the expected range for the ciliary beat. The details of this step can be found in our previous publication. The structural images were first masked based on pixel intensity to eliminate the background pixels without tissue. For each spatial pixel corresponding to the tissue, the pixel intensity over time was analyzed through a fast Fourier transform (FFT) over the first 128 images to obtain the frequency amplitude spectrum. To distinguish pixels corresponding to cilia, we applied a cutoff threshold based on spectral amplitude set as an average amplitude plus three standard deviations from the frequency window of 30–35 Hz, where no ciliary beating is expected, and the variations could be assumed to be background noise. Pixels that contain the frequency peaks over the threshold within the window of 2–15 Hz were counted as the pixels corresponding to cilia. For each pixel, the highest peak on the spectrum indicated the cilia beat frequency at that location.

A MW analysis could only be performed across one dominant frequency at a time. We selected the frequencies for analysis based on the dominant representation and clustering pixels of specific frequencies within regions of interest. Another binary mask was created to include all pixels where the selected frequency was represented in the spectrum over a set threshold, regardless of whether this frequency corresponded to the spectral peak. For OCT imaging, the threshold was set as the average spectral amplitude from the frequency window of 30–35 Hz plus 10 times the standard deviation. For bright-field video microscopy, the threshold was set as the average spectral amplitude from the frequency window of 30–35 Hz plus 0.7 times the standard deviation. The phase at the selected frequency was mapped over all pixels that remained after the masking. CBF analysis, frequency thresholding, and phase mapping steps were repeated for the selected frequency with a sliding window over time, which introduced the time component to phase mapping for spatiotemporal analysis of wavefront propagation. The wavefront displacement in space over time was used to determine the cilia metachronal wave velocity.

E. Software

OCT imaging, data acquisition, and export were performed through LabVIEW (National Instruments Corporation)-based custom software. Acquisition of bright-field video microscopy data was performed using ZEN software (Zeiss). Data processing was

Author Manuscript Author Manuscript Author Manuscript Author Manuscript

performed using custom codes written in MATLAB (MathWorks, Inc.). Data visualizations and volumetric renderings, and supplementary videos were created using Imaris software (Oxford Instruments plc).

F. Statistical Analysis

The Pearson correlation coefficient test was used to compare the paired metachronal wave velocity measurements acquired with two modalities, the bright-field video microscopy and OCT, with a significance level of $\alpha = 0.05$. Brown-Forsythe and Welch analysis of variance tests were applied to determine whether there is significant difference between metachronal wave velocity measurements at three temperature settings.

Supplementary Material

Refer to Web version on PubMed Central for supplementary material.

Funding.

National Institutes of Health (F32HD110222, R01EB027099, R35GM142953).

Acknowledgment.

The authors would like to thank Yupei Lin and Michaela McCown (Baylor College of Medicine) for their advice on data presentation. Parts of Fig. 1 were created with BioRender.com.

Data availability.

The dynamics cilia MW propagation analysis was performed using custom codes implemented in MATLAB R2021a (MathWorks Inc.). These codes are available from the corresponding author upon reasonable request. All data needed to evaluate the conclusions are present in the paper and/or the supplementary materials. Additional data related to this paper may be requested from the authors.

REFERENCES

1. Elgeti J, Winkler RG, and Gompper G, “Physics of microswimmers–single particle motion and collective behavior: a review,” Rep. Prog. Phys 78, 056601 (2015). [PubMed: 25919479]
2. Tamm SL, “Ciliary motion in paramecium: a scanning electron microscope study,” J. Cell Biol 55, 250 (1972). [PubMed: 4569410]
3. Gilpin W, Prakash VN, and Prakash M, “Vortex arrays and ciliary tangles underlie the feeding–swimming trade-off in starfish larvae,” Nat. Phys 13, 380–386 (2017).
4. Nonaka S, Shiratori H, Saijoh Y, and Hamada H, “Determination of left-right patterning of the mouse embryo by artificial nodal flow,” Nature 418, 96–99 (2002). [PubMed: 12097914]
5. Ramirez-San Juan GR, Mathijssen AJ, He M, Jan L, Marshall W, and Prakash M, “Multi-scale spatial heterogeneity enhances particle clearance in airway ciliary arrays,” Nat. Phys 16, 958–964 (2020). [PubMed: 35937969]
6. Faubel R, Westendorf C, Bodenschatz E, and Eichele G, “Cilia-based flow network in the brain ventricles,” Science 353, 176–178 (2016). [PubMed: 27387952]
7. Lyons RA, Saridogan E, and Djahanbakhch O, “The reproductive significance of human Fallopian tube cilia,” Hum. Reprod. Update 12, 363–372 (2006). [PubMed: 16565155]

Author Manuscript Author Manuscript Author Manuscript Author Manuscript

8. Gu H, Boehler Q, Cui H, Secchi E, Savorana G, De Marco C, Gervasoni S, Peyron Q, Huang TY, Pane S, Hirt AM, Ahmed D, and Nelson BJ, "Magnetic cilia carpets with programmable metachronal waves," Nat. Commun 11, 2637 (2020). [PubMed: 32457457]
9. Elgeti J and Gompper G, "Emergence of metachronal waves in cilia arrays," Proc. Natl. Acad. Sci. USA 110, 4470–4475 (2013). [PubMed: 23487771]
10. Vilfan A and Julicher F, "Hydrodynamic flow patterns and synchronization of beating cilia," Phys. Rev. Lett 96, 058102 (2006). [PubMed: 16486996]
11. Wan KY and Goldstein RE, "Coordinated beating of algal flagella is mediated by basal coupling," Proc. Natl. Acad. Sci. USA 113, E2784–E2793 (2016). [PubMed: 27140605]
12. Quaranta G, Aubin-Tam ME, and Tam D, "Hydrodynamics versus intracellular coupling in the synchronization of eukaryotic flagella," Phys. Rev. Lett 115, 238101 (2015). [PubMed: 26684142]
13. Meng F, Bennett RR, Uchida N, and Golestanian R, "Conditions for metachronal coordination in arrays of model cilia," Proc. Natl. Acad. Sci. USA 118, e2102828118 (2021).
14. Chakrabarti B, Furthauer S, and Shelley MJ, "A multiscale biophysical model gives quantized metachronal waves in a lattice of beating cilia," Proc. Natl. Acad. Sci. USA 119, e2113539119 (2022).
15. Milana E, Zhang R, Vetrano MR, Peerlinck S, De Volder M, Onck PR, Reynaerts D, and Gorissen B, "Metachronal patterns in artificial cilia for low Reynolds number fluid propulsion," Sci. Adv 6, eabd2508 (2020).
16. Dong X, Lum GZ, Hu W, Zhang R, Ren Z, Onck PR, and Sitti M, "Bioinspired cilia arrays with programmable nonreciprocal motion and metachronal coordination," Sci. Adv 6, eabc9323 (2020).
17. Milla CE, "The evolving spectrum of ciliopathies and respiratory disease," Curr. Opin. Pediatr 28, 339 (2016). [PubMed: 27070443]
18. Ferkol TW and Leigh MW, "Ciliopathies: the central role of cilia in a spectrum of pediatric disorders," J. Pediatr 160, 366–371 (2012). [PubMed: 22177992]
19. Ringers C, Olstad EW, and Jurisch-Yaksi N, "The role of motile cilia in the development and physiology of the nervous system," Philos. Trans. R. Soc. B 375, 20190156 (2019).
20. Li Y, Klena NT, Gabriel GC, et al. , "Global genetic analysis in mice unveils central role for cilia in congenital heart disease," Nature 521, 520–524 (2015). [PubMed: 25807483]
21. Bustamante-Marin XM, Yin WN, Sears PR, Werner ME, Brotslaw EJ, Mitchell BJ, Jania CM, Zeman KL, Rogers TD, Herring LE, Refabert L, Thomas L, Amselem S, Escudier E, Legendre M, Grubb BR, Knowles MR, Zariwala MA, and Ostrowski LE, "Lack of GAS2L2 causes PCD by impairing cilia orientation and mucociliary clearance," Am. J. Hum. Genet 104, 229–245 (2019). [PubMed: 30665704]
22. Mee L, Honkala H, Kopra O, Vesa J, Finnila S, Visapaa I, Sang TK, Jackson GR, Salonen R, Kestila M, and Peltonen L, "Hydrolethalus syndrome is caused by a missense mutation in a novel gene HYLS1," Hum. Mol. Genet 14, 1475–1488 (2005). [PubMed: 15843405]
23. Reiter JF and Leroux MR, "Genes and molecular pathways underpinning ciliopathies," Nat. Rev. Mol. Cell Biol 18, 533–547 (2017). [PubMed: 28698599]
24. Hyland RM and Brody SL, "Impact of motile ciliopathies on human development and clinical consequences in the newborn," Cells 11, 125 (2021). [PubMed: 35011687]
25. Honore I and Burgel PR, "Primary ciliary dyskinesia in adults," Rev. Mal. Respir 33, 165–189 (2016). [PubMed: 26654126]
26. Knowles MR, Daniels LA, Davis SD, Zariwala MA, and Leigh MW, "Primary ciliary dyskinesia. Recent advances in diagnostics, genetics, and characterization of clinical disease," Am. J. Respir. Crit. Care Med 188, 913–922 (2013). [PubMed: 23796196]
27. Yuan S, Wang Z, Peng H, Ward SM, Hennig GW, Zheng H, and Yan W, "Oviductal motile cilia are essential for oocyte pickup but dispensable for sperm and embryo transport," Proc. Natl. Acad. Sci. USA 118, e2102940118 (2021).
28. Niwa S, Nakajima K, Miki H, Minato Y, Wang D, and Hirokawa N, "KIF19A is a microtubule-depolymerizing kinesin for ciliary length control," Dev. Cell 23, 1167–1175 (2012). [PubMed: 23168168]

Author Manuscript Author Manuscript Author Manuscript Author Manuscript

29. Shi D, Komatsu K, Hirao M, Toyooka Y, Koyama H, Tissir F, Goffinet AM, Uemura T, and Fujimori T, “Celsr1 is required for the generation of polarity at multiple levels of the mouse oviduct,” Development 141, 4558–4568 (2014). [PubMed: 25406397]
30. Inhorn MC and Patrizio P, “Infertility around the globe: new thinking on gender, reproductive technologies and global movements in the 21st century,” Hum. Reprod. Update 21, 411–426 (2015). [PubMed: 25801630]
31. Wang S and Larina IV, “In vivo dynamic 3D imaging of oocytes and embryos in the mouse oviduct,” Cell Rep. 36, 109382 (2021). [PubMed: 34260920]
32. Wang S, Burton JC, Behringer RR, and Larina IV, “In vivo micro-scale tomography of ciliary behavior in the mammalian oviduct,” Sci. Rep 5, 13216 (2015). [PubMed: 26279472]
33. Zhao W, Zhu Q, Yan M, Li C, Yuan J, Qin G, and Zhang J, “Levonorgestrel decreases cilia beat frequency of human fallopian tubes and rat oviducts without changing morphological structure,” Clin. Exp. Pharmacol. Physiol 42, 171–178 (2015). [PubMed: 25399777]
34. Liao S, Ho J, Tang F, and O WS, “Adrenomedullin increases ciliary beat frequency and decreases muscular contraction in the rat oviduct,” Reproduction 141, 367–372 (2010). [PubMed: 21173072]
35. Ryser M, Burn A, Wessel T, Frenz M, and Ricka J, “Functional imaging of mucociliary phenomena: high-speed digital reflection contrast microscopy,” Eur. Biophys. J 37, 35–54 (2007). [PubMed: 18027008]
36. Liu L, Gardecki JA, Nadkarni SK, Toussaint JD, Yagi Y, Bouma BE, and Tearney GJ, “Imaging the subcellular structure of human coronary atherosclerosis using micro–optical coherence tomography,” Nat. Med 17, 1010–1014 (2011). [PubMed: 21743452]
37. Liu L, Chu KK, Houser GH, Diephuis BJ, Li Y, Wilsterman EJ, Shastry S, Dierksen G, Birket SE, Mazur M, Byan-Parker S, Grizzle WE, Sorscher EJ, Rowe SM, and Tearney GJ, “Method for quantitative study of airway functional microanatomy using micro-optical coherence tomography,” PLOS ONE 8, e54473 (2013). [PubMed: 23372732]
38. Solomon GM, Francis R, Chu KK, Birket SE, Gabriel G, Trombley JE, Lemke KL, Klena N, Turner B, Tearney GJ, Lo CW, and Rowe SM, “Assessment of ciliary phenotype in primary ciliary dyskinesia by micro-optical coherence tomography,” JCI Insight 2, e91702 (2017). [PubMed: 28289722]
39. Birket SE, Chu KK, Houser GH, Liu L, Fernandez CM, Solomon GM, Lin V, Shastry S, Mazur M, Sloane PA, Hanes J, Grizzle WE, Sorscher EJ, Tearney GJ, and Rowe SM, “Combination therapy with cystic fibrosis transmembrane conductance regulator modulators augment the airway functional microanatomy,” Am. J. Physiol 310, L928–L939 (2016).
40. Birket SE, Chu KK, Liu L, Houser GH, Diephuis BJ, Wilsterman EJ, Dierksen G, Mazur M, Shastry S, Li Y, Watson JD, Smith AT, Schuster BS, Hanes J, Grizzle WE, Sorscher EJ, Tearney GJ, and Rowe SM, “A functional anatomic defect of the cystic fibrosis airway,” Am. J. Respir. Crit. Care Med 190, 421–432 (2014). [PubMed: 25029666]
41. Raju SV, Lin VY, Liu L, McNicholas CM, Karki S, Sloane PA, Tang L, Jackson PL, Wang W, Wilson L, Macon KJ, Mazur M, Kappes JC, DeLucas LJ, Barnes S, Kirk K, Tearney GJ, and Rowe SM, “The cystic fibrosis transmembrane conductance regulator potentiator ivacaftor augments mucociliary clearance abrogating cystic fibrosis transmembrane conductance regulator inhibition by cigarette smoke,” Am. J. Respir. Cell Mol. Biol 56, 99–108 (2016).
42. Cui D, Chu KK, Yin B, Ford TN, Hyun C, Leung HM, Gardecki JA, Solomon GM, Birket SE, Liu L, Rowe SM, and Tearney GJ, “Flexible, high-resolution micro-optical coherence tomography endo-bronchial probe toward in vivo imaging of cilia,” Opt. Lett 42, 867–870 (2017). [PubMed: 28198885]
43. Chu KK, Unglert C, Ford TN, Cui D, Carruth RW, Singh K, Liu L, Birket SE, Solomon GM, Rowe SM, and Tearney GJ, “In vivo imaging of airway cilia and mucus clearance with micro-optical coherence tomography,” Biomed. Opt. Express 7, 2494–2505 (2016). [PubMed: 27446685]
44. Leung HM, Birket SE, Hyun C, Ford TN, Cui D, Solomon GM, Shei RJ, Adewale AT, Lenzie AR, Fernandez-Petty CM, Zheng H, Palermo JH, Cho DY, Woodworth BA, Yonker LM, Hurley BP, Rowe SM, and Tearney GJ, “Intranasal micro-optical coherence tomography imaging for cystic fibrosis studies,” Sci. Transl. Med 11, eaav3505 (2019). [PubMed: 31391319]

Author Manuscript Author Manuscript Author Manuscript Author Manuscript

45. Oldenburg AL, Chhetri RK, Hill DB, and Button B, “Monitoring airway mucus flow and ciliary activity with optical coherence tomography,” Biomed. Opt. Express 3, 1978–1992 (2012). [PubMed: 23024894]
46. Ling Y, Yao X, Gamm UA, Arteaga-Solis E, Emala CW, Choma MA, and Hendon CP, “Ex vivo visualization of human ciliated epithelium and quantitative analysis of induced flow dynamics by using optical coherence tomography,” Lasers Surg. Med 49, 270–279 (2017). [PubMed: 28231402]
47. Groux K, Verschueren A, Nanteau C, Clemencon M, Fink M, Sahel JA, Boccara C, Paques M, Reichman S, and Grieve K, “Dynamic full-field optical coherence tomography allows live imaging of retinal pigment epithelium stress model,” Commun. Biol 5, 575 (2022). [PubMed: 35688936]
48. Scholler J, Groux K, Goureau O, Sahel JA, Fink M, Reichman S, Boccara C, and Grieve K, “Dynamic full-field optical coherence tomography: 3D live-imaging of retinal organoids,” Light Sci. Appl 9, 140 (2020). [PubMed: 32864115]
49. Jing JC, Chen JJ, Chou L, Wong BJ, and Chen Z, “Visualization and detection of ciliary beating pattern and frequency in the upper airway using phase resolved Doppler optical coherence tomography,” Sci. Rep 7, 8522 (2017). [PubMed: 28819309]
50. He Y, Jing JC, Qu Y, Wong BJ, and Chen Z, “Spatial mapping of tracheal ciliary beat frequency using real time phase-resolved Doppler spectrally encoded interferometric microscopy,” ACS Photon. 7, 128–134 (2020).
51. He Y, Qu Y, Jing JC, and Chen Z, “Characterization of oviduct ciliary beat frequency using real time phase resolved Doppler spectrally encoded interferometric microscopy,” Biomed. Opt. Express 10, 5650–5659 (2019). [PubMed: 31799037]
52. Miao Y, Jing JC, Chou L, Zhu Z, Wong BJF, and Chen Z, “Phase-resolved dynamic wavefront imaging of cilia metachronal waves,” Quant. Imag. Med. Surg 13, 2364–2375 (2023).
53. Huang BK and Choma MA, “Microscale imaging of cilia-driven fluid flow,” Cell. Mol. Life Sci 72, 1095–1113 (2015). [PubMed: 25417211]
54. Jonas S, Bhattacharya D, Khokha MK, and Choma MA, “Microfluidic characterization of cilia-driven fluid flow using optical coherence tomography-based particle tracking velocimetry,” Biomed. Opt. Express 2, 2022–2034 (2011). [PubMed: 21750777]
55. Huang BK, Gamm UA, Bhandari V, Khokha MK, and Choma MA, “Three-dimensional, three-vector-component velocimetry of cilia-driven fluid flow using correlation-based approaches in optical coherence tomography,” Biomed. Opt. Express 6, 3515–3538 (2015). [PubMed: 26417520]
56. Zhou KC, Huang BK, Gamm UA, Bhandari V, Khokha MK, and Choma MA, “Particle streak velocimetry-optical coherence tomography: a novel method for multidimensional imaging of microscale fluid flows,” Biomed. Opt. Express 7, 1590–1603 (2016). [PubMed: 27375926]
57. Brendan KH, Ute AG, Stephan J, Mustafa KKMD, and Michael ACMD, “Quantitative optical coherence tomography imaging of intermediate flow defect phenotypes in ciliary physiology and pathophysiology,” J. Biomed. Opt 20, 030502 (2015). [PubMed: 25751026]
58. Ute Alice G, Brendan KH, Mansoor Ali S, Xuchen Z, Vineet Bhandari MD, and Michael ACMD, “Quantifying hyperoxia-mediated damage to mammalian respiratory cilia-driven fluid flow using particle tracking velocimetry optical coherence tomography,” J. Biomed. Opt 20, 080505 (2015). [PubMed: 26308164]
59. Scopulovic L, Francis D, Pandzic E, and Francis R, “Quantifying cilia beat frequency using high-speed video microscopy: assessing frame rate requirements when imaging different ciliated tissues,” Physiol. Rep 10, e15349 (2022). [PubMed: 35678028]
60. Shi D, Komatsu K, Uemura T, and Fujimori T, “Analysis of ciliary beat frequency and ovum transport ability in the mouse oviduct,” Genes Cells 16, 282–290 (2011). [PubMed: 21294816]
61. Bylander A, Nutu M, Wellander R, Goksor M, Billig H, and Larsson DG, “Rapid effects of progesterone on ciliary beat frequency in the mouse fallopian tube,” Reprod. Biol. Endocrinol 8, 48 (2010). [PubMed: 20470431]
62. Lyons RA, Djahanbakhch O, Mahmood T, Saridogan E, Sattar S, Sheaff MT, Naftalin AA, and Chenoy R, “Fallopian tube ciliary beat frequency in relation to the stage of menstrual cycle and anatomical site,” Hum. Reprod 17, 584–588 (2002). [PubMed: 11870107]

Author Manuscript Author Manuscript Author Manuscript Author Manuscript

63. Ringers C, Bialonski S, Ege M, Solovev A, Hansen JN, Jeong I, Friedrich BM, and Jurisch-Yaksi N, “Novel analytical tools reveal that local synchronization of cilia coincides with tissue-scale metachronal waves in zebrafish multiciliated epithelia,” Elife 12, e77701 (2023). [PubMed: 36700548]
64. Moore EL, Wang S, and Larina IV, “Staging mouse preimplantation development in vivo using optical coherence microscopy,” J. Biophoton 12, e201800364 (2019).
65. Wang S, Syed R, Grishina OA, and Larina IV, “Prolonged in vivo functional assessment of the mouse oviduct using optical coherence tomography through a dorsal imaging window,” J. Biophoton 11, e201700316 (2018).
66. Keenan M, Tate TH, Kieu K, Black JF, Utzinger U, and Barton JK, “Design and characterization of a combined OCT and wide field imaging falloposcope for ovarian cancer detection,” Biomed. Opt. Express 8, 124–136 (2017). [PubMed: 28101406]
67. Madore WJ, De Montigny E, Deschenes A, Benboujja F, Leduc M, Mes-Masson AM, Provencher DM, Rahimi K, Boudoux C, and Godbout N, “Morphologic three-dimensional scanning of fallopian tubes to assist ovarian cancer diagnosis,” J. Biomed. Opt 22, 76012 (2017). [PubMed: 28727868]
68. Wijesundara K, Zdanski C, Kimbell J, Price H, Iftimia N, and Oldenburg AL, “Quantitative upper airway endoscopy with swept-source anatomical optical coherence tomography,” Biomed. Opt. Express 5, 788–799 (2014). [PubMed: 24688814]
69. McLaughlin RA, Noble PB, and Sampson DD, “Optical coherence tomography in respiratory science and medicine: from airways to alveoli,” Physiology 29, 369–380 (2014). [PubMed: 25180266]
70. Jing JC, Chou L, Su E, Wong BJF, and Chen Z, “Anatomically correct visualization of the human upper airway using a high-speed long range optical coherence tomography system with an integrated positioning sensor,” Sci. Rep 6, 39443 (2016). [PubMed: 27991580]
71. Syed SH, Larin KV, Dickinson ME, and Larina IV, “Optical coherence tomography for high-resolution imaging of mouse development in utero,” J. Biomed. Opt 16, 046004 (2011). [PubMed: 21529073]
72. Raghunathan R, Liu C-H, Kouka A, Singh M, Miranda RC, and Larin KV, “Dose-response analysis of microvasculature changes in the murine fetal brain and the maternal extremities due to prenatal ethanol exposure,” J. Biomed. Opt 25, 1–13 (2020).
73. Leopold PL, O’Mahony MJ, Lian XJ, Tilley AE, Harvey B-G, and Crystal RG, “Smoking is associated with shortened airway cilia,” PloS One 4, e8157 (2009). [PubMed: 20016779]
74. Stanley P, Wilson R, Greenstone M, MacWilliam L, and Cole P, “Effect of cigarette smoking on nasal mucociliary clearance and ciliary beat frequency,” Thorax 41, 519–523 (1986). [PubMed: 3787531]
75. Klein T and Huber R, “High-speed OCT light sources and systems [Invited],” Biomed. Opt. Express 8, 828–859 (2017). [PubMed: 28270988]
76. Mitran SM, “Metachronal wave formation in a model of pulmonary cilia,” Computers & Structures 85, 763–774 (2007). [PubMed: 19169426]
77. Berlinger F, Gauci M, and Nagpal R, “Implicit coordination for 3D underwater collective behaviors in a fish-inspired robot swarm,” Sci. Robot 6, eabd8668 (2021).
78. Drotman D, Jadhav S, Sharp D, Chan C, and Tolley MT, “Electronics-free pneumatic circuits for controlling soft-legged robots,” Sci. Robot 6, eabd8668 (2021).
79. Zhang S, Cui Z, Wang Y, and den Toonder J, “Metachronal μ-cilia for on-chip integrated pumps and climbing robots,” ACS Appl. Mater. Interfaces 13, 20845–20857 (2021). [PubMed: 33884875]
80. Bryan MT, Martin EL, Pac A, Gilbert AD, and Ogrin FY, “Metachronal waves in magnetic micro-robotic paddles for artificial cilia,” Commun. Mater 2, 1–7 (2021).

Author Manuscript Author Manuscript Author Manuscript Author Manuscript

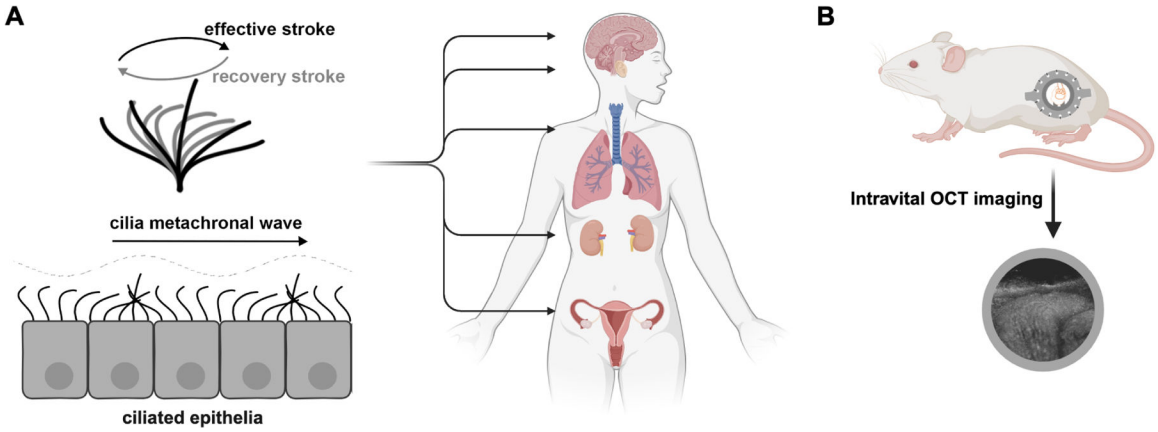

Fig. 1.

Physiology and investigation of motile cilia. A: Motile cilia are hairlike structures that beat in coordination to produce waves (metachronal waves) along epithelial surfaces. Motile cilia are critical for the physiological function of multiple organs including the brain, the middle ear, the respiratory tract, the kidney, and the fallopian tube. B: An intravital OCT imaging approach to study cilia dynamics in the mouse fallopian tube *in vivo*.

Author Manuscript
Author Manuscript
Author Manuscript
Author Manuscript

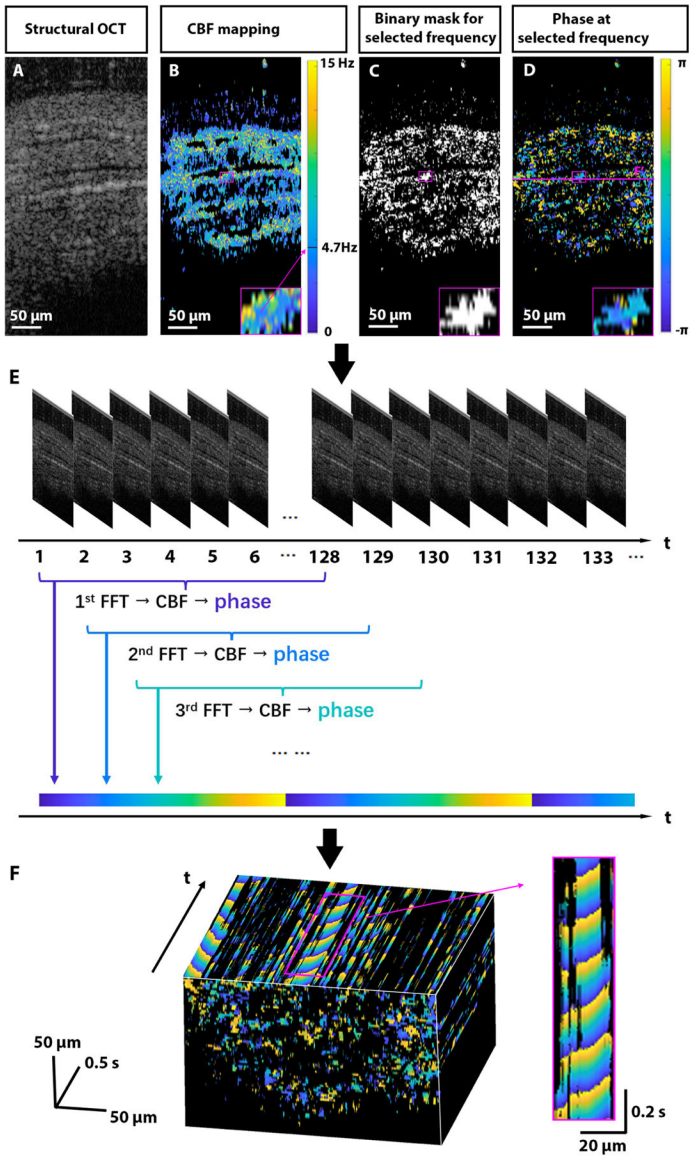

Fig. 2.

Proposed algorithm for visualization and quantitative analysis of cilia metachronal wave. The presented example is an intact extracted mouse oviduct with highly ciliated luminal longitudinal grooves. The imaging plane was oriented along the grooves to ensure metachronal wave orientation within that plane. A: Time-lapse structural OCT imaging is performed through the ciliated sample. B: Pixel-wise FFT analysis is performed on the OCT time-lapse to reveal the CBF in corresponding pixels after thresholding. The fragment used for metachronal wave analysis is enlarged in the inlet, showing the dominant frequency of 4.7 Hz, which was selected for further analysis. C: The binary mask for the dominant frequency is created to include all pixels where this frequency amplitude is over the threshold. D: The corresponding FFT phases are mapped. The dashed line indicates the location of the cross-section and metachronal wave visualization in panel F. E: The FFT and

phase mapping for the same dominant frequency is repeated as a sliding window over time, F: revealing metachronal wave propagation over space and time.

Author Manuscript Author Manuscript Author Manuscript Author Manuscript

Author Manuscript Author Manuscript Author Manuscript Author Manuscript

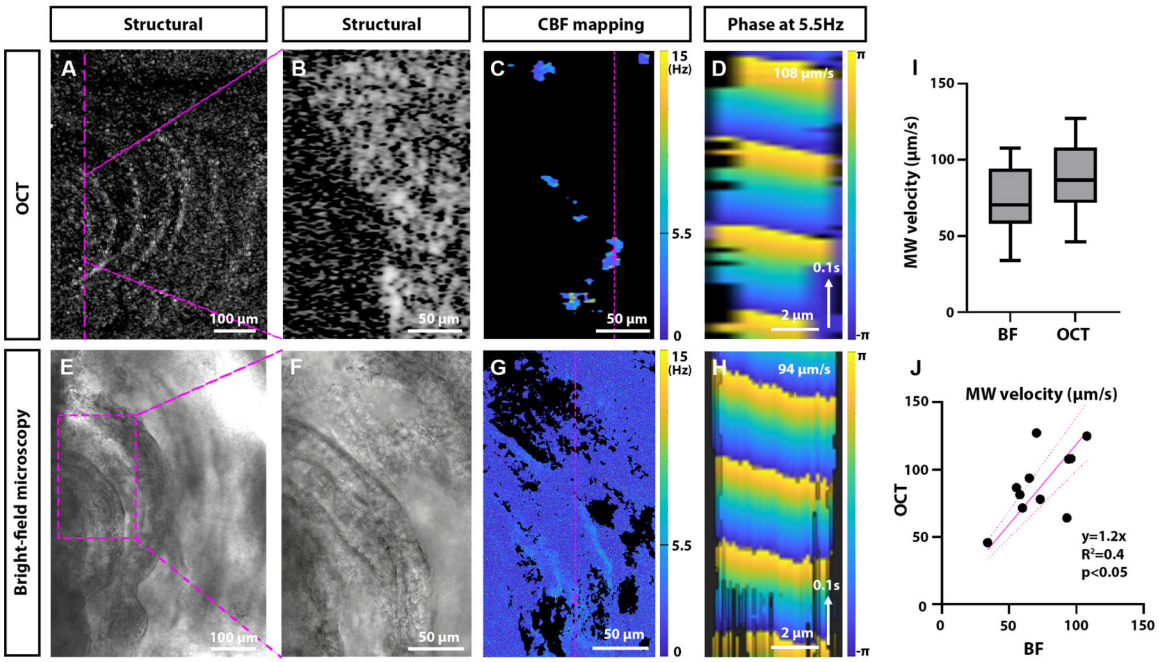

Fig. 3.

Validation of OCT 2D + time metachronal wave mapping. Sample comparison of the metachronal wave velocity measurement in the same spatial location of an extracted fallopian tube sample with OCT (A–D) and bright-field video microscopy (E–H). A: Top view of the overall volumetric structural rendering of the sample acquired with OCT. The location of the imaging plane and the fragment for future analysis shown in B and C are labeled with magenta lines. B: Corresponding zoom-in fragment of the in-depth OCT structural B-scan (top is on the left), and C: CBF mapping. The magenta line and notches indicate the fragment analyzed in panel D. D: The spatiotemporal phase wavefront reconstruction with OCT at 5.5 Hz reveals metachronal wave propagation at 107 mm/s. E: Large field of view (10X) bright-field microscopy image of the same sample. F: Higher-magnification view (40X) of the fragment labeled in E with the magenta box. G: Corresponding CBF mapping. The magenta line and notches indicate the fragment analyzed in panel H. H: The spatiotemporal cilia metachronal wavefront reconstruction with bright-field microscopy at 5.5 Hz reveals metachronal wave propagation at 94 mm/s. I: Comparison of metachronal wave velocity measurements with bright-field microscopy and OCT (N = 11 for each group). J: Pearson correlation coefficient test for paired measurements demonstrates a statistically significant correlation between the metachronal wave velocity measurements with two modalities (N = 11).

Author Manuscript Author Manuscript Author Manuscript Author Manuscript

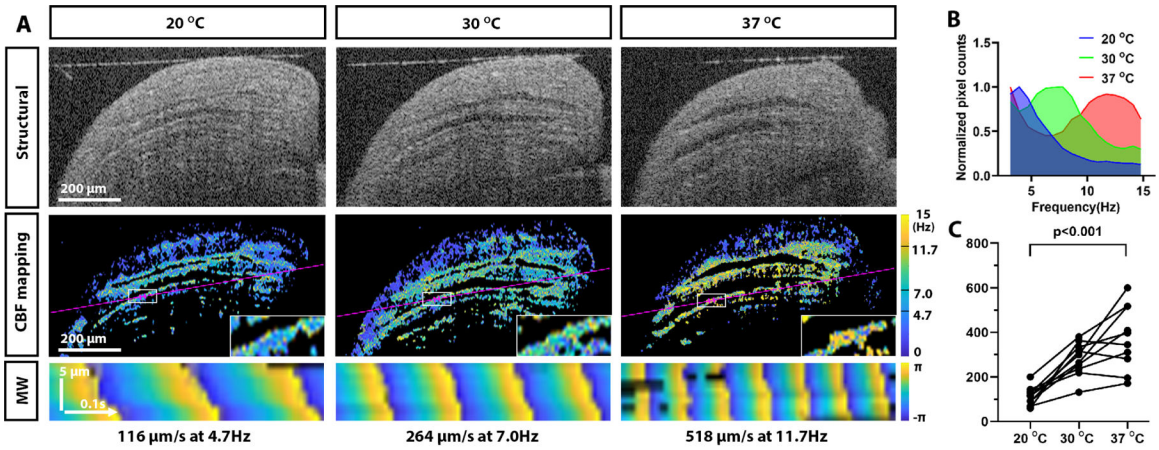

Fig. 4.

Cilia metachronal wave velocity increases with temperature. A: Structural OCT images of the same location of a mouse fallopian tube imaged *ex vivo* at different temperatures are shown in the top row. Corresponding CBF maps are shown in the middle row; the areas used for the metachronal wave analysis are marked with white rectangles and enlarged inlets for each panel. The magenta lines indicate the positions for the metachronal wavefront maps in the bottom row. B: The histogram of CBFs calculated over the whole area of the images in A shifts toward higher frequencies with an increase in temperature. C: The cilia metachronal wave velocity increases with temperature. N = 10 regions from three independent experimental samples. $p < 0.001$.

Author Manuscript Author Manuscript Author Manuscript Author Manuscript

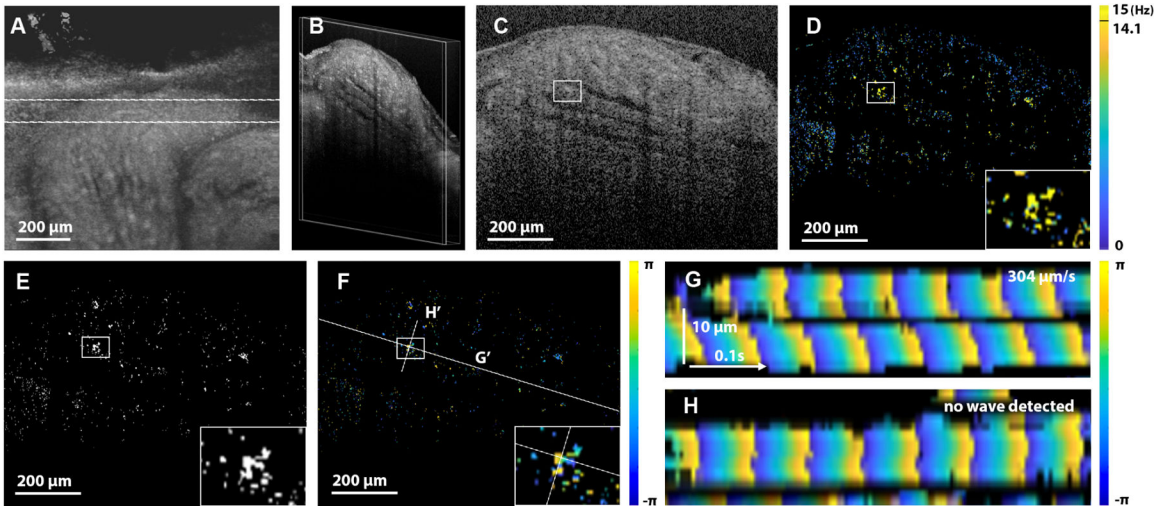

Fig. 5.

In vivo OCT quantitative analysis of cilia metachronal wave in mouse fallopian tube. A: Top view of the 3D OCT of the fallopian tube. The lines indicate the location of the 2D+time dataset covering the turn of the fallopian tube, where the luminal grooves are parallel to the scanning plane. B: Volumetric view of the imaged slice with longitudinal grooves. C: An in-depth slice through the ridges of the luminal grooves, selected for further analysis. Corresponding D: CBF mapping, E: spectral mask for CBF of 14.1 Hz, and F: phase mapping over the whole field of view. The insets highlight the region of interest, and the lines indicate the positions, where the metachronal wavefront was reconstructed. G and H: Spatiotemporal reconstruction of the metachronal wavefront along and perpendicular to the grove, respectively, shows that the metachronal wave propagated along the grove at 304 μm/s.

Author Manuscript Author Manuscript Author Manuscript Author Manuscript

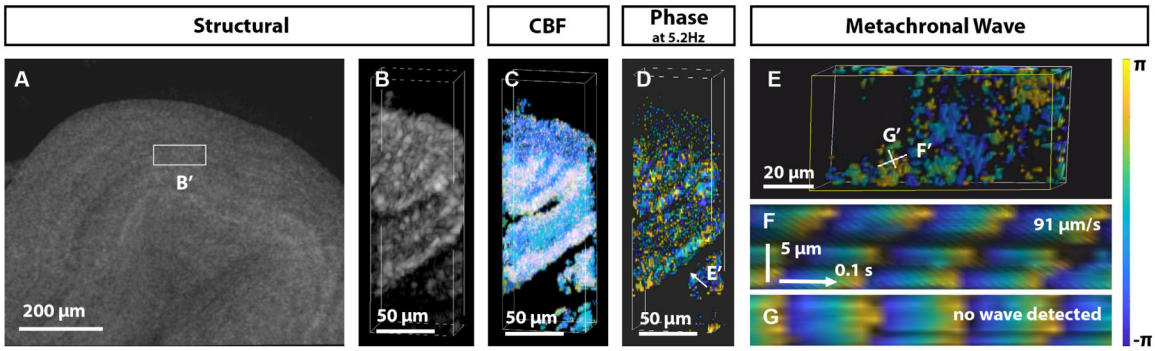

Fig. 6.

Direct volumetric imaging of cilia metachronal wave propagation in the mouse fallopian tube. A: Large view of the 3D OCT rendering of the fallopian tube ampulla. The region used for 3D+time imaging is labeled. B: Volumetric view of structural OCT of the selected region with ciliated oviductal grooves, C: corresponding frequency mapping, and D: phase at 5.2 Hz dominant frequency. E: Phase distribution over the surface of one of the grooves viewed from the direction indicated in D. F: Plotting the phase along the line labeled in E over time reveals metachronal wavefront propagation at 91 µm/s, G while the orthogonal orientation does not show any identifiable waves.